Phase Behavior of Magnetic Colloid−Polymer Mixtures: 2. A Magnetic Sensing Coil Study

G. A. van Ewijk, G. J. Vroege,* and B. W. M. Kuipers

Van't Hoff Laboratory for Physical and Colloid Chemistry, Debye Institute, Utrecht University, Padualaan 8, 3584 CH Utrecht, The Netherlands

Received July 17, 2001. In Final Form: October 9, 2001

The effects of dipolar interaction and isotropic attraction on the phase behavior of ferrofluids are separately investigated by studying a ferrofluid, containing oleic acid grafted magnetite particles, mixed with nonadsorbing polymer. The presence of polymer causes an effective isotropic attraction (depletion attraction) between the magnetic particles, with a strength determined by the polymer concentration. The magnetic interaction was modified by applying a magnetic field. A phase diagram is measured using a magnetic sensing coil, which allows measurement of the magnetic particle concentration in the separate phases without disturbing the sample. Moreover, it is shown that the sensing coil in principle also allows determination of the polymer concentration in the separate phases. In practice, however, this determination in complicated by the fact that phase separation can cause significant fractionation: particle sizes in the dilute phase were up to 33% lower than those in the unfractionated ferrofluid. In the absence of polymer, the ferrofluid is stable at all concentrations and field strengths. Phase separation, even in zero field, is observed above polymer concentrations of, typically, 50 g L^{-1}. Applying a magnetic field of 28 kA m^{-1} lowers the amount of polymer at which the ferrofluid destabilizes by approximately 20%. Excess oleic acid at a concentration of 160 g L^{-1} was also found to induce phase separation.

1. Introduction

Ferrofluids are colloidal dispersions of (mostly) spherical ferro- or ferrimagnetic particles in a nonmagnetic solvent. Because of its monodomain nature, each particle has a permanent magnetic dipole moment. The—on average—attractive nature of the dipolar interaction between the particles can lower a ferrofluid's thermodynamic stability against separation into a dilute (gas) phase and a concentrated (liquid) phase. Moreover, the average strength of attraction can be increased by applying a magnetic field, thereby further promoting phase separation.

Phase separation in ferrofluids has been experimentally observed under several conditions.[1] In charge-stabilized ferrofluids, addition of salt can induce gas−liquid phase separation.[1] Sterically (oleic acid) stabilized ferrofluids can be destabilized in zero field by decreasing the solvent quality[1] or adding nonadsorbing polymer.[2] And phase separation induced by a magnetic field is probably the most frequently reported instability.[3−6]

In at least three of these cases, isotropic attraction plays an important role in the instability. In this respect, the system of a ferrofluid containing nonadsorbing polymer is of particular interest: the polymer induces an effective isotropic attraction ("depletion attraction") between the magnetic colloids, which can be varied independently of the magnetic attraction. This is therefore a suitable system for studying the influence of both isotropic and anisotropic interaction on the phase behavior of ferrofluids.

The aim of our study is to experimentally investigate the phase behavior of mixtures of a high-quality ferrofluid and nonadsorbing polymer, both in zero-field and in an applied magnetic field. The ferrofluid consists of oleic acid stabilized magnetite particles with a size of roughly 10 nm. The stability of ferrofluids is often studied using optical microscopy, which directly reveals the nature (gas, liquid, and/or solid) of the coexisting phases. In principle, it also allows determination of the interfacial tension and the difference in susceptibility between dilute and concentrated phases.[7] In this study, we employ a different technique: a magnetic sensing coil[8−11] is used, which allows the direct determination of the susceptibility at any height in a sample tube with high accuracy. This instrument gives information about the volumes and susceptibilities (and hence the concentrations) of all phases in a nondestructive way. Moreover, it is shown that, at least in principle, the polymer concentration in each separate phase can be obtained indirectly from sensing coil measurements.

Without polymer, the ferrofluid remains homogeneous at all field strengths and concentrations. In zero field, the ferrofluid−polymer mixture separates into two phases with different ferrofluid concentrations if enough polymer is added. Applying a magnetic field of 28 kA m^{-1} reduces the polymer concentration at which the mixture destabilizes with about 20%. This agrees quite well with the theoretical predictions made in a previous paper.[12] Due to polydispersity, phase separation also brings about size

* Corresponding author. E-mail: g.j.vroege@chem.uu.nl.

(1) Dubois, E.; Cabuil, V.; Boue, F.; Bacri, J.-C.; Perzynski, R. *Prog. Colloid Polym. Sci.* **1997**, *104*, 1173.
(2) Cabuil, V.; Perzynski, R.; Bastide, J. *Prog. Colloid Polym. Sci.* **1994**, *97*, 75.
(3) Pshenichnikov, A. F.; Shurubor, I. Y. *Izv. Akad. Nauk SSSR, Ser. Fiz.* **1987**, *51*, 1081.
(4) Rosensweig, R. E.; Popplewell, J. In *Electromagnetic Forces and Applications*; Tani, J., Takagi, T., Eds.; Elsevier Science Publishers: Amsterdam, 1992; p 83.
(5) Horng, H.-E.; Hong, C.-Y.; Yeung, W. B.; Yang, H.-C. *Appl. Opt.* **1998**, *37*, 2674.
(6) Hong, C.-Y.; Jang, I. J.; Horng, H. E.; Hsu, C. J.; Yao, Y. D.; Yang, H. C. *J. Appl. Phys.* **1997**, *81*, 4275.
(7) Bacri, J. C.; Salin, D., *J. Phys.* **1982**, *43*, L649.
(8) Peterson, E. A.; Krueger, D. A. *J. Colloid Interface Sci.* **1977**, *62*, 24.
(9) Chantrell, R. W.; Sidhu, J.; Bissell, P. R.; Bates, P. A. *J. Appl. Phys.* **1982**, *53*, 8341.
(10) Bissell, P. R.; Chantrell, R. W.; Spratt, G. W. D.; Bates, P. A.; O'Grady, K. D. *IEEE Trans. Magn.* **1984**, *20*, 1738.
(11) Dababneh, M. S.; Ayoub, N. Y. *IEEE Trans. Magn.* **1995**, *31*, 4178.
(12) van Ewijk, G. A.; Vroege, G. J. *Langmuir* **2001**, *18*, 377.

10.1021/la011117j CCC: $22.00
Published on Web 12/27/2001

fractionation. Although this affects the sensing coil measurements, the measured phase diagram still shows many features of the predicted diagram.

Apart from its fundamental interest, the results of this study may also be applicable in optical applications of phase separated ferrofluids,[5] since addition of nonadsorbing polymer enhances the control over the volumes and concentrations of the two phases.

2. Experimental Section

2.1. Materials. A high-quality magnetic fluid, coded FFR, was obtained from Politehnica Universita of Timişoara (Romania). It consisted of Fe_3O_4 particles obtained from chemical precipitation, grafted with purified oleic acid (9-*Z*-octadecanoic acid).[13] Excess oleic acid was removed by repeated precipitation/redispersion cycles. Any aggregates were removed by filtration and magnetic sedimentation. The particles were dispersed in cyclohexane (analytical grade).

Poly(dimethylsiloxane) (ACBR, $M_w = 41.5$ kg mol^{-1}, radius of gyration ≈ 8.5 nm), PDMS, was used as a nonadsorbing polymer. Oleic acid (Acros, "extra pure", 97%) was used to investigate the influence of excess surfactant on the stability of FFR.

2.2. Characterization. Transmission electron microscopy (TEM) photographs were taken on a Philips CM10 electron microscope and analyzed with IBAS (an electronic image analysis system).

Magnetization measurements were carried out on a MicroMag 2900 AGM (alternating gradient magnetometer, Princeton Measurements Corp.). Samples were contained in small glass cups with internal dimensions of $4 \times 3 \times 0.4$ mm, which were sealed by gluing a small cover glass over the open end. All measurements were performed at room temperature. The saturation magnetization and diamagnetic susceptibility were determined by fitting the magnetization curve at high fields (up to 1.2×10^6 A m^{-1}) with the Langevin function[14,15] and an added diamagnetic contribution

$$M = M_s\left\{\coth(\alpha) - \frac{1}{\alpha}\right\} + \chi_{dia}H; \qquad \alpha = \frac{\mu_o m H}{kT} \tag{1}$$

where M_s is the saturation magnetization of the sample, χ_{dia} the diamagnetic susceptibility, H the applied field strength, m the magnetic moment of particles, μ_0 the permeability of vacuum, and kT the thermal energy. The initial susceptibility χ_i was obtained by determining the slope of the magnetization curve at applied fields below 10^3 A m^{-1}. The magnetic core size d_M of particles was then calculated using the slope of (1) in the low-field approximation

$$\chi_i = M_s\frac{\mu_o m}{3kT} + \chi_{dia} = M_s\frac{\mu_o M_{s,Fe_3O_4}\pi d_M^{\,3}}{18kT} + \chi_{dia} \tag{2}$$

where M_{s,Fe_3O_4} is the saturation magnetization of bulk Fe_3O_4 (4.8×10^5 A m^{-1}). To minimize the influence of magnetic interaction between magnetite particles, eq 2 was only used for measurements on samples with a concentration of magnetic material below 10 g L^{-1}.

Small-angle X-ray scattering (SAXS) experiments were done at the DUBBLE beamline (BM26) at the European Synchrotron Radiation Facility in Grenoble. Scattering experiments were conducted on dilute samples ($\phi < 1\%$). The radius of gyration, R_g, was calculated using the low q approximation of the scattering intensity of a dilute dispersion:[16] $\ln[I(q)/I(0)] = -R_g^2q^2/3$, where $q = (4\pi/\lambda_0)\sin(\theta/2)$ is the scattering vector, θ the scattering angle, and $\lambda_0 = 1.03$ Å the wavelength of incident radiation.

(13) Bica, D. *Rom. Rep. Phys.* **1995**, *47*, 265.
(14) Jacobs, I. S.; Bean, C. P. In *Magnetism, a treatise on modern theory and materials*; Rado, G. T., Suhl, H., Eds.; Academic Press: New York, 1963; Vol. III, p 271.
(15) Rosensweig, R. E. *Ferrohydrodynamics*; Cambridge University Press: Cambridge, 1985.
(16) Porod, G. In *Small-Angle X-ray Scattering*; Glatter, O., Kratky, O., Eds.; Academic Press: London, 1982; p 17.

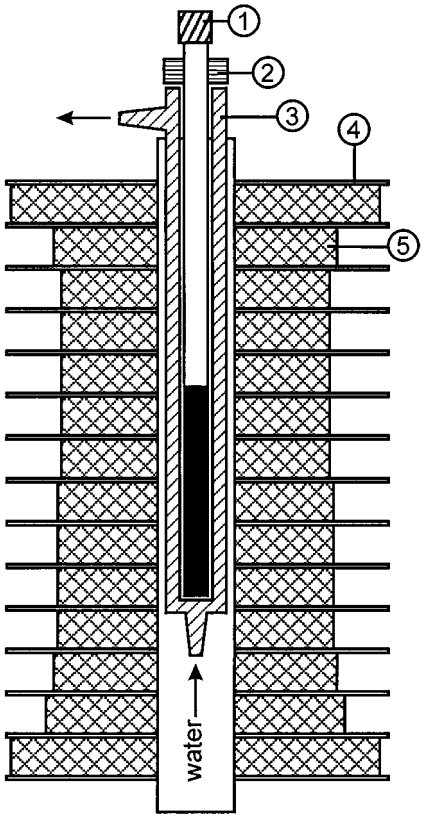

Figure 1. Schematic drawing of the setup used for phase separation experiments: (1) sample tube; (2) magnetic sensing coil; (3) water-cooled thermostat; (4) copper cooling plates; (5) copper windings.

The mass density ρ of a dispersion was measured with an Anton Paar DMA 5000 densitometer. Combined with the mass concentration c this yields the density of dry particles ρ_{dry}

$$\rho_{dry} = \frac{c\rho_{solvent}}{c + \rho_{solvent} - \rho} \tag{3}$$

2.3. Experimental Setup for Phase Separation Experiments. All phase separation experiments were carried out in the setup, which is schematically drawn in Figure 1. Briefly, the setup consists of a long cylindrical electromagnet, capable of generating magnetic fields up to 30 kA m^{-1}. In the electromagnet's core, a thermostat controls the temperature of the sample with an accuracy of 0.1 °C. The concentration of magnetic particles is measured by moving the sample tube through a magnetic sensing coil.

The electromagnet is a coil made of copper wire (1.08 mm) wound around a PVC tube in 11-mm segments, separated by 1 mm thick copper cooling plates. The plates allow for fast radial transport of heat to the perimeter of the coil. Heat is dissipated by air convection, but the cooling plates allow for forced cooling in the future, enabling higher magnetic field strengths than currently attainable.

A heterogeneous distribution of the number of windings per segment was chosen, with the following criteria in mind. First, the volume over which the field can be considered homogeneous should be as large as possible. This requires an increasing number of windings toward both ends of the coil. Second, because phase separation experiments rely on the gravitational settling of concentrated droplets or aggregates, magnetic field gradients that obstruct settling must be absent. The maximum gradient ∇H can be calculated by comparing the gravitational and magnetic force on a droplet with volume V, density ρ, and magnetization M

$$\mu_0 VM\nabla H < V(\rho - \rho_s)g \tag{4}$$

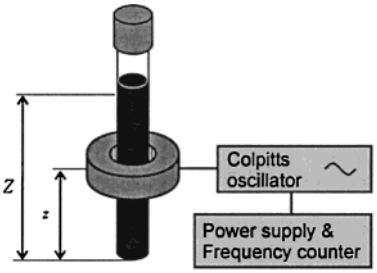

Figure 2. Schematic drawing of the susceptibility meter setup.

ρ_s is the solvent density, μ_0 the permeability of vacuum, and g the Earth's gravitational acceleration. Assuming equal densities of the grafting layer and the solvent, the density difference in eq 4 becomes $\varphi_m(\rho_m - \rho_s)$, with ρ_m the density of the magnetic material and φ_m the volume fraction of magnetic material. To obtain the smallest estimate for ∇H, we take the droplet to be fully magnetized, i.e., $M = \varphi_m M_{s,m}$ ($M_{s,m}$ is the bulk saturation magnetization of the magnetic material). Equation 4 then becomes

$$\nabla H < \frac{(\rho_m - \rho_s)g}{\mu_0 M_{s,m}} \tag{5}$$

For magnetite, the upward gradient should therefore be less than 7×10^4 A m^{-2} everywhere in the sample. In our setup, the number of windings was distributed in a way that should give a gradient of 10^4 A m^{-2} downward at the maximum field of 3×10^4 A m^{-1}. Because both the gradient and the sample length are small, the homogeneity of the field is only slightly affected.

2.4. The Magnetic Sensing Coil. The magnetic sensing coil is similar to the one described by Peterson et al.[8] The coil is part of a Colpitts oscillation circuit, which in turn is connected to a frequency counter (HAMEG HM8021-3) and a dc power supply (technical details can be found in ref 17). The coil produces an oscillating magnetic field with an amplitude of about 100 A m^{-1} and a base frequency f_0 close to 1 MHz. Inserting a ferrofluid sample into the coil changes the self-inductance of the coil and with it the frequency of the oscillator. The frequency change Δf is related to the initial magnetic susceptibility χ_i of the sample, which is the response of the magnetization M to a (small) external field H. At low concentrations, χ_i depends linearly on the particle number density n

$$\chi_i \equiv \left(\frac{\partial M}{\partial H}\right)_{H=0} = n\,\frac{\mu_0}{3kT}\langle m^2\rangle \tag{6}$$

where $\langle\ \rangle$ denotes a number average. At higher concentrations the linearity is lost, but measuring χ is still a convenient method to obtain the magnetic particle concentration. The accuracy of the sensing coil is about 10^{-4}, which corresponds to a magnetic particle concentration of roughly 0.1 g L^{-1}.

Measurements with the magnetic sensing coil consist of moving a sample in 1-mm steps through the coil and measuring Δf after each step. To see how the profile $\Delta f(z)$ is related to the susceptibility profile $\chi(Z)$ of the sample, we first calculate the change in the self-inductance, ΔL, of the coil when a ferrofluid sample is inserted into it as shown in Figure 2. The change in self-inductance is, by definition, proportional to the change of magnetic flux, $\Delta\Phi$, through the coil due to the presence of magnetized ferrofluid. If the sample is considered as a stack of thin ferrofluid disks, the contribution to $\Delta\Phi$ of each disk is proportional to its susceptibility $\chi(Z)$ and depends on its position $(z - Z)$ with respect to the coil. The contribution of all disks is the convolution integral

$$\Delta L(z) \propto \int_{-\infty}^{+\infty} \chi(Z)\, r(z - Z)\, \mathrm{d}Z \tag{7}$$

where $r(z - Z)$ is a (bell-shaped) response function which only depends on the geometry of the coil and the width of the sample tube. Equation 7 implies that sharp changes in the $\chi(Z)$ profile appear smeared out in the $\Delta L(z)$ profile. Using $L \propto f^{-2}$ for this oscillator[11] yields the desired relation between $\Delta f(z)$ and $\chi(Z)$

$$F(z) \equiv \left(\frac{f_0}{f_0 + \Delta f(z)}\right)^2 - 1 \propto \int_{-\infty}^{+\infty} \chi(Z)\, r(z - Z)\, \mathrm{d}Z \tag{8}$$

where $F(z)$ is a measurable quantity which is proportional to $\Delta L(z)$. For the simple case of a height-independent susceptibility, eq 8 reduces to $F \propto \chi$, which was used in earlier publications.[8,11]

The $F(z)$ profile of a step-shaped susceptibility profile that is zero at $Z < Z_{step}$ and nonzero and constant at $Z > Z_{step}$ and can be written in the form

$$F(z) \propto \chi R(z - Z_{step}) \tag{9}$$

$$R(z) = \int_0^{+\infty} r(z - Z)\, \mathrm{d}Z$$

The function $R(z)$ depends only on the geometry of the coil and the internal diameter of the sample tube. Once $R(z)$ is known, eq 9 can be used to locate phase boundaries in macroscopically phase separated samples, provided the interface between two phases is flat and sharp. The positions Z_{step1}, Z_{step2}, ... are found by fitting the measured $F(z)$ profile with a sum of convoluted step profiles (eq 9).

2.5. Sample Preparation for Sensing Coil Measurements. Samples for measurements with the sensing coil were contained in cylindrical glass tubes (internal diameter = 6 mm) with a flat bottom, which could be sealed with a screwcap.

The (overall) concentrations of magnetic material, PDMS, or excess oleic acid in a sample were calculated from the total weight of the sample, the weights of the materials dispersed in it, and the densities of the materials and the solvent, assuming that all volumes are additive. The weights of dispersed materials were determined before measurements. To this purpose, some FFR was dried under flowing nitrogen and weighed. Then, if applicable, weighed amounts of PDMS or oleic acid were added. Finally, the materials were dispersed in cyclohexane under vigorous shaking.

Measurements over a concentration range were performed by adding solvent or evaporating solvent under a gentle nitrogen stream. After each dilution or concentration step, concentrations of dispersed materials were calculated as described above.

All measurements were done at 296 K.

2.6. Calibration of the Sensing Coil. The relation between the ferrofluid concentration and F (from eq 8) was measured for concentrations between 50 and 600 g L^{-1}. A single sample was used, the concentration of which was increased as described in the previous section.

To test if the presence of nonadsorbing polymer affects the relation between F and concentration, the calibration was repeated with samples to which PDMS was added. Four samples with different polymer/colloid mass ratios were used.

The convoluted step profile $R(z)$ (eq 9) was determined by measuring the $F(z)$ profile of a dilute, homogeneous ferrofluid.

2.7. Phase Separation Experiments. Dilute colloid−polymer mixtures were prepared as described in section 2.5. Each sample was concentrated a little and mixed thoroughly, after which it was left to stand for at least 1 day. A concentration profile was then recorded by moving the sample in 1-mm steps through the coil and measuring F after each such step. If the phase separation experiment took place in an applied magnetic field, the field was switched off just before the profile was recorded and the tube was treated very gently to minimize distortion of the profile, which is metastable in that case. The procedure of concentrating and measuring was repeated several times to obtain measurements over a range of concentrations.

The position of a concentration step in the sample, if any, was determined by fitting the concentration profile with the sum of two convoluted step functions (eq 9), one corresponding to the bottom and the other to the interface between the concentrated and dilute phase. Note that the second step represents the difference between the concentrated and the dilute phase and therefore has a negative amplitude.

(17) van Ewijk, G. A. Phase behavior of mixtures of magnetic colloids and nonadsorbing polymer. Ph.D. Thesis, Utrecht University, 2001.

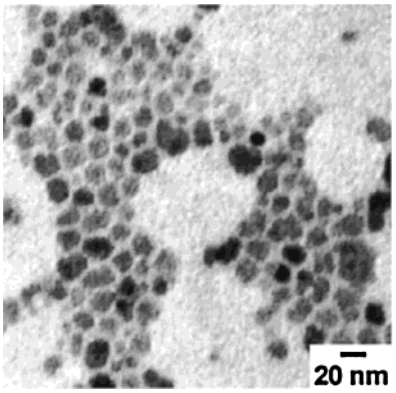

Figure 3. TEM picture of FFR.

A few phase separation experiments were also carried out on ferrofluids to which excess oleic acid was added.

2.8. Size Fractionation. Because our samples are polydisperse, the size of magnetic particles in demixed samples is expected to be different in both phases. Therefore, size fractionation in phase-separated samples was examined after the phase separation experiments. Starting from their most concentrated state, samples were stepwise diluted by adding cyclohexane and left to stand for at least 1 day. After each dilution step, the size of particles in the upper phase was measured by taking about 5 μL of that phase, diluting it with cyclohexane, and analyzing it using magnetometry (section 2.2).

3. Results and Discussion

3.1. Magnetic Fluid Characteristics. A TEM picture of FFR is shown in Figure 3. The average diameter of the particle cores d_{TEM} is 9.1 nm ($\sigma = 26\%$). The diameter d_M obtained from magnetization measurements is 11.3 nm. Note that $d_M^3 = \langle d_m^6\rangle/\langle d_m^3\rangle$[18,19] ($d_m$ is the magnetic core size of one particle), so polydispersity strongly increases the diameter found with eq 2 and makes d_M larger than d_{TEM}. This difference between d_M and d_{TEM} is reduced by the presence of a nonmagnetic surface layer.[15,19]

An estimate of the dipole−dipole interaction parameter $\lambda = \mu_0 m^2/(4\pi kTd^3)$ and the reduced field strength $\alpha = \mu_0 mH/(kT)$ can be made, using $d = d_{TEM} + 2 \times 2$ nm (the thickness of the oleic acid layer is roughly 2 nm) and $m = (\pi/6)d_M^3 M_{s,Fe_3O_4}$. The value for m actually overestimates the average value, since d_M^3 is significantly larger than $\langle d_m^3\rangle$. With the high estimate of m, we find $\lambda = 1.4$ and $\alpha = 3.1$ at $H = 28$ kA m^{-1}.

The ferrofluid was stable against sedimentation: no sediment was formed even after a year. However, absence of a sediment in ferrofluid samples is insufficient to conclude that clusters are absent:[20] sediments only form when the gravitational length[21] $l_g = kT/Nmg$ (N = number of particles in a cluster, m = mass of a single particle, corrected for buoyancy $\approx 3 \times 10^{-21}$ kg, g = Earth's gravity constant) is less than, say, a millimeter. This condition is only satisfied for clusters of about 100 particles or more; smaller clusters remain dispersed because their thermal energy is larger than their gravitational energy. The presence of clusters was therefore investigated using SAXS.

Figure 4 shows the Guinier plot of a dilute sample of FFR at small scattering vectors. A straight line fits the scattering curve well. The linearity of the Guinier plot up to the smallest q value demonstrates that clusters are absent. It is in agreement with dichroism and rheological measurements done with the same kind of ferrofluid.[22] The slope of the curve gives a radius of gyration of 6.5 nm. For homogeneous spherical particles, the physical particle diameter $d = 2R_g(5/3)^{1/2} = 16.8$ nm. The difference between the SAXS diameter and the TEM diameter can be largely attributed to polydispersity. If particle sizes are log-normally distributed, then[18]

$$\frac{d_{SAXS}}{d_{TEM}} = \frac{(\langle d^8\rangle/\langle d^6\rangle)^{1/2}}{\langle d\rangle} = \frac{\exp(7\sigma^2)}{\exp(\sigma^2/2)} \qquad (10)$$

Substituting $\langle d\rangle = 9.1$ nm and $\sigma = 0.26$ in (10) yields $d_{SAXS} = 14.1$ nm.

The mass density ρ_{dry} of dried ferrofluid was found to be 2900 kg m^{-3}. The lower density compared to bulk magnetite is due to the presence of the oleic acid layer around the particles.

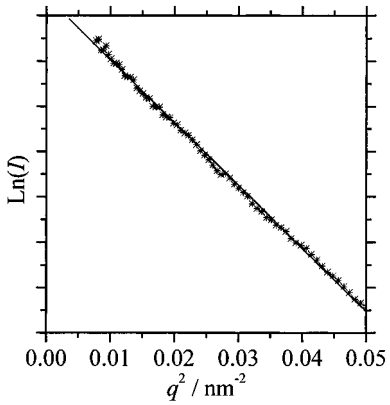

Figure 4. Guinier plot of SAXS measurement of FFR. The linearity up to small q indicates that clusters are absent.

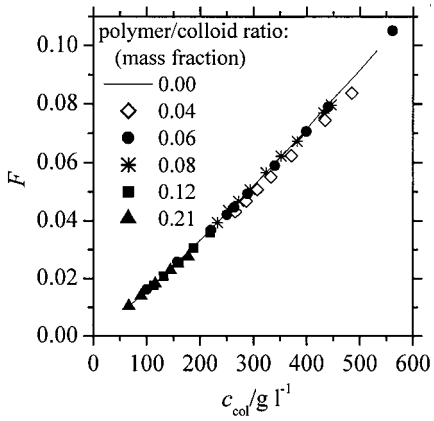

Figure 5. Calibration curves of magnetic sensing coil. Polymer has negligible influence on the susceptibility.

3.2. Calibration of the Sensing Coil. The susceptibility as a function of concentration is shown in Figure 5. The data show a small but consistent deviation from a linear relation owing to mutual magnetic interaction between the colloids. Samples with different polymer concentrations all coincide, so the presence of polymer does not affect the measurement of the magnetic particle concentration.

(18) Cabuil, V.; Perzynski, R. In *Magnetic Fluids and Applications Handbook*; Berkovski, B., Eds.; Begell House: New York, 1996.
(19) Pshenichnikov, A. F.; Mekhonoshin, V. V.; Lebedev, A. V. *J. Magn. Magn. Mater.* **1996**, *161*, 94.
(20) Scholten, P. C. *Chem. Eng. Commun.* **1988**, *67*, 331.
(21) Degiorgio, V.; Piazza, R.; Bellini, T. In *Observation, prediction and simulation of phase transitions in complex fluids*; Baus, M., Rull, L. F., Ryckaert, J.-P., Eds.; Kluwer Academic Publishers: Dordrecht, 1995.
(22) Vékás, L.; Rasa, M.; Bica, D. *J. Colloid Interface Sci.* **2000**, *231*, 247.

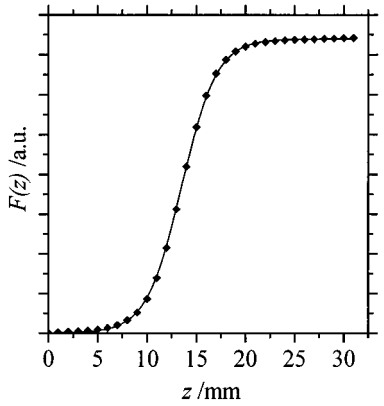

Figure 6. Convoluted step profile: (◆) measurements; (—) fit with eq 11.

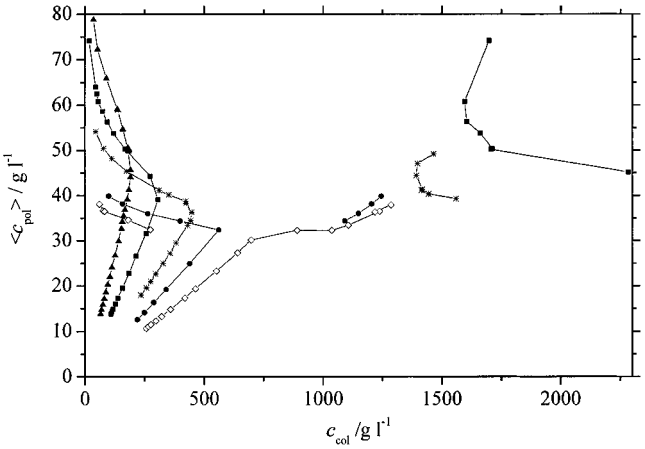

Figure 7. Experimental phase diagram of magnetic fluid (FFR) containing nonadsorbing polymer. Samples with fixed polymer/colloid ratios are concentrated, giving straight lines in the single-phase region and a separate "gas" and "liquid" branch in the two-phase region. Note that the polymer concentration $\langle c_{pol} \rangle$ is the calculated overall concentration in the entire sample.

A measured convoluted step profile is shown in Figure 6. Using the empirical equation

$$R(z - Z_{step}) = \frac{1}{1 + \exp\left[-\frac{(z - Z_{step})}{w}\right]} \qquad (11)$$

where w the extent of smearing (in our setup, $w = 1.76$ mm), the measured profile could be very well described with eq 9 (see Figure 6). From (11) it can be derived that 95% of the signal comes from the area within 7 mm from the center of the coil.

3.3. Phase Separation Experiments in Zero Field. Figure 7 shows the experimental phase diagram of FFR mixed with PDMS. The concentration of magnetic particles, c_{col}, was obtained from F using the calibration curve 5. The magnetic sensing coil cannot measure the polymer concentration in each phase. Therefore, in the experimental diagram (Figure 7) the *overall* polymer concentration, $\langle c_{pol} \rangle$, was plotted on the vertical axis. The overall polymer concentration was calculated from the weight of polymer added to the sample, as described in section 2.5.

Of some samples the concentration line was also measured in the opposite direction, i.e., by diluting the sample. These measurements coincided exactly with the points measured by concentrating, showing that the instability is reversible and reproducible.

A typical susceptibility profile of a two-phase sample and a fit with the sum of two convoluted step profiles are

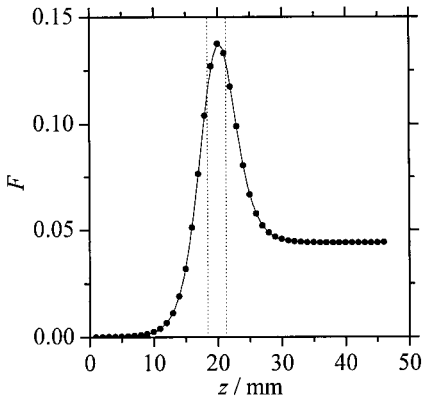

Figure 8. Typical susceptibility profile of a phase separated sample: (●) measurements; (—) fitted profile; (· · ·) positions of concentration steps.

shown in Figure 8. The dotted lines represent the positions of the bottom of the tube and the interface between the phases. Measurements and the fitted curve are in excellent agreement, suggesting that the interface is sharp. Susceptibility profiles never showed significant changes after 1 day, so it is probably an equilibrium state we are observing. In most samples the dilute phase occupied the largest part of the sample volume. The susceptibility of this phase could therefore be measured directly without interference from boundaries such as the fluid meniscus. The concentrated phase was in many cases so thin and concentrated that demagnetization[23] was expected to hinder the direct determination of the susceptibility. Therefore, the concentration of magnetic particles was obtained indirectly from the thickness of this phase. Conservation of mass states that $M_{total} = M_{gas} + M_{liquid}$. This gives us the magnetic particle concentration in the concentrated phase

$$c_{liquid} = \frac{M_{total} - c_{gas}V_{gas}}{V_{liquid}} \qquad (12)$$

All points on the liquid lines in Figure 7 were calculated this way.

A phase diagram similar to Figure 7 was also measured using a lower quality ferrofluid (FOC1) with practically the same size distribution as FFR.[17] Oleic acid was removed from FOC1, but no measures were taken to decrease the level of aggregation. This had a profound influence on the stability. For instance, whereas the FFR with a concentration of $c_{col} = 100$ g L^{-1} is stable at polymer concentrations up to 60 g L^{-1}, FOC1 with $c_{col} = 100$ g L^{-1} destabilizes already at 25 g L^{-1} polymer. This indicates that the phase behavior of ferrofluids strongly depends on its microstructural properties.

The effect of excess oleic acid on the stability of FFR was also investigated. It was found that a sample with $c_{col} = 290$ g L^{-1} ($\phi = 0.10$) destabilized at excess oleic acid concentrations above 160 g L^{-1}, which is higher than the value of 58 g L^{-1} predicted in our previous paper,[12] but too low to explain it as a bad solvent effect. Considering the 28 vol % of ethanol that is needed to destabilize a cylohexane-based ferrofluid[1] and the 50 vol % of the less polar pentanol,[17] the even less polar oleic acid is expected to destabilize a cyclohexane ferrofluid at even higher concentrations. The value of 18 vol % of oleic acid (=160 g L^{-1}) indicates that oleic acid is likely to act as a depletion agent rather than a bad solvent.

(23) Kittel, C. *Introduction to Solid State Physics*, 3rd ed.; John Wiley & Sons: New York, 1953.

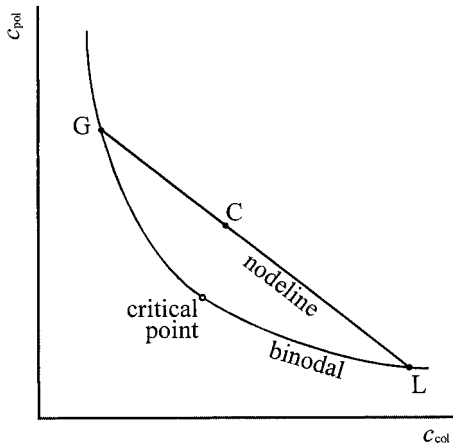

Figure 9. General phase diagram of colloid−polymer mixtures.

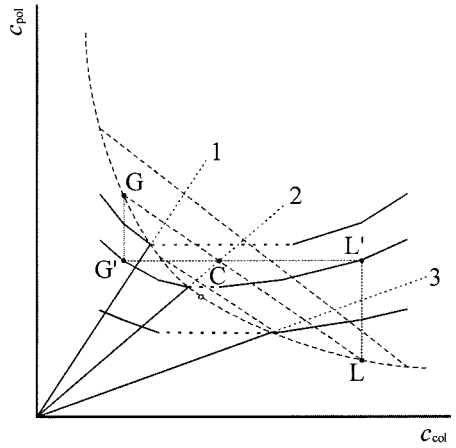

Figure 10. Construction of the experimental phase diagram from the theoretical phase diagram of colloid−polymer mixtures.

3.4. Interpretation of the Zero Field Phase Diagram. The polymer in a colloid−polymer mixture induces an effective attraction between the colloidal particles, which can give rise to phase separation.[24] A general phase diagram of a monodisperse colloid−polymer mixture is sketched in Figure 9; c_{col} and c_{pol} refer to the concentrations of colloids and polymers, respectively. A mixture having a composition *C* or any other composition on the nodeline will demix into two phases G and L, G (a colloidal "gas") being poor in colloids and rich in polymer and L (a colloidal "liquid") being rich in colloids and poor in polymer. Such a colloidal gas−liquid coexistence is expected for polymer/colloid size ratios larger than 0.3.[25]

Because the sensing coil cannot measure the polymer concentration in each phase directly, the experimental phase diagram (Figure 7) is plotted in a different representation than Figure 9. Therefore, to compare the theoretical and experimental diagrams, we construct in Figure 10 what the experimental diagram would look like for the phase diagram given in Figure 9. The lines labeled 1, 2, and 3 are three samples whose concentrations are varied by adding or removing solvent. This changes the overall composition but leaves the colloid/polymer ratio unaffected; hence, the concentration lines are straight lines through the origin. Beyond the coexistence curve, phase separation takes place and a concentration line splits into a gas line and a liquid line. Depending on the position with respect to the critical point, there is a discontinuous transition from the concentration line to either the gas or the liquid line and a continuous transition to the other line. As an example, the construction of two points in the experimental diagram is shown in Figure 10. A sample with initial composition *C* demixes into two phases having compositions G and L. In the experimental diagram G and L are shifted vertically to G′ and L′ such that their polymer concentration equals the overall polymer concentration, which is just the polymer concentration in *C*.

The constructed diagram contains several features that can also be found in the measured diagram (Figure 7). The discontinuity in going from the concentration line to either the gas or the liquid line is seen both theoretically and experimentally. The critical point of FFR should be close to the point where the sample with the second lowest polymer/colloid ratio becomes unstable, i.e., around $c_{col} = 550$ and $c_{pol} = 32$ g L^{-1}. Deviations from the expected behavior are also present. In samples with high polymer/colloid ratios, a gradual transition from the concentration line to the gas line is found, whereas a sharp transition was expected. Also, the liquid lines of these samples show a peculiar feature, namely, a decreasing colloid concentration with increasing polymer concentration. This behavior is explained in section 3.6.

3.5. Phase Separation Experiments in an Applied Field. At all concentrations tested (from 5% to 30% by vol), the ferrofluid sample without added polymer remained homogeneous in a magnetic field of 30 kA m^{-1}. This seems to contradict several literature reports on the phase separation of similar systems,[3−6] where magnetic fluids generally destabilize below fields of 10 kA m^{-1}. However, as Pshenichnikov has experimentally demonstrated[3] and Ivanov has argued,[26] phase separation in these systems is strongly promoted by the presence of a small fraction of large particles. The system used here has a lower polydispersity than those reported elsewhere (with the exception of ref 4) and apparently lacks the large particles causing phase separation. In addition, the SAXS measurements show that clusters are absent, which may also explain the higher stability. Furthermore, the presence of free oleic acid may be disadvantageous for ferrofluid stability.[12,27] Contrary to the ferrofluids used in refs 5 and 6 our ferrofluid underwent several precipitation/redispersion cycles to remove free oleic acid. Refs 3 and 4 do not contain information from which the presence or absence of free oleic acid may be derived.

The effect of an applied magnetic field on the stability of colloid−polymer mixtures can be seen in Figure 11. Samples with a composition far from the zero-field binodal remain homogeneous even in the highest magnetic field. At compositions closer to the zero field binodal, samples phase separate if the magnetic field strength exceeds a certain threshold value. When the zero-field binodal is approached, the threshold field strength is reduced (and eventually vanishes), and the reduction of the magnetic particle concentration in the upper phase becomes stronger.

In Figure 12, a part of the zero-field phase diagram is plotted together with the phase diagram in a constant field of 28 kA m^{-1}. Three samples with polymer/colloid mass ratios of 0.039, 0.057, and 0.13 were used. The magnetic field lowers the binodal to roughly 20% lower polymer concentrations. This agrees well with the mean field calculations[12] for $q = 0.5$, $\alpha = 3$, and $\lambda \approx 1$, and

(24) Asakura, S.; Oosawa, F. *J. Polym. Sci.* **1958**, *XXXIII*, 183.
(25) Lekkerkerker, H. N. W.; Poon, W. C.-K.; Pusey, P. N.; Stroobants, A.; Warren, P. B. *Europhys. Lett.* **1992**, *20*, 559.
(26) Ivanov, A. O. *Colloid J.* **1995**, *57*, 321.
(27) Dubois, E. Stabilité des solutions colloidales magnétiques (ferrofluides) [In French]. Ph.D. Thesis, Universite Pierre et Marie Curie, Paris, 1997.

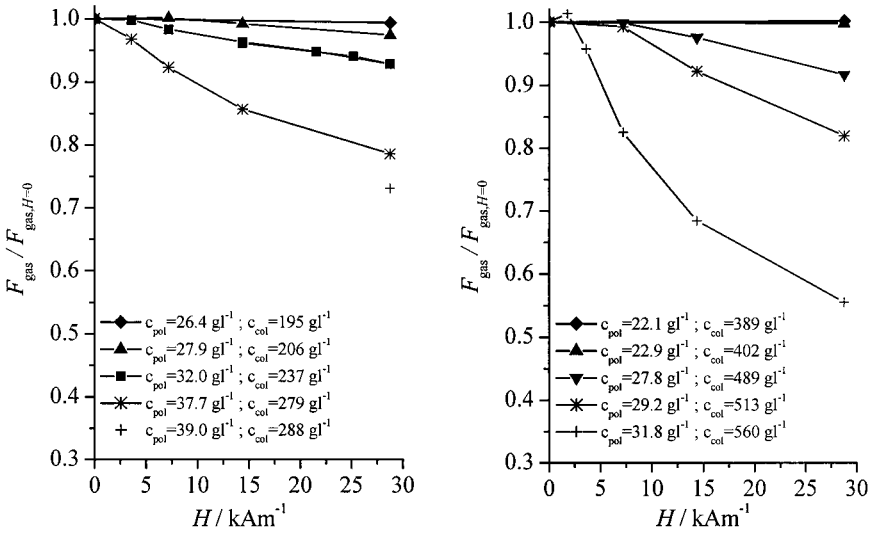

Figure 11. Influence of an external magnetic field on the stability of PDMS/Fe_3O_4 mixtures with a high (left) or low (right) polymer/colloid ratio. The plots shows the susceptibility of the dilute phase at a given field strength relative to the susceptibility of the dilute phase without a field.

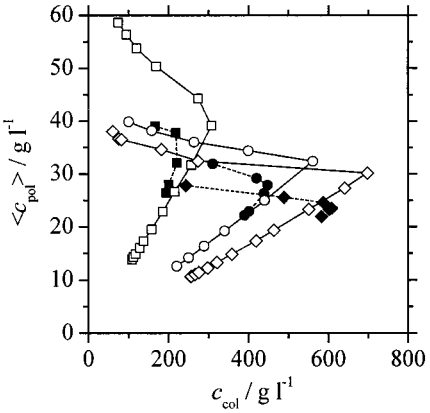

Figure 12. Comparison of concentration lines in a constant magnetic field of 28 kA m^{-1} (closed symbols) with lines in zero field (open symbols).

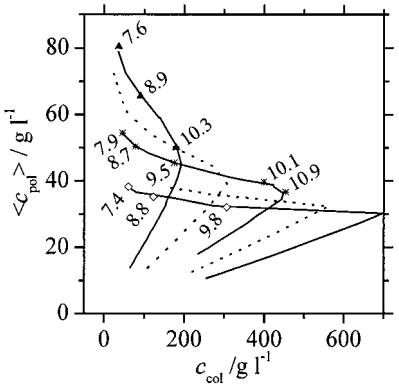

Figure 13. Fractionation upon phase separation in zero field. Numbers in plot area represent particle sizes in nanometers, measured with magnetization measurements (eq 2). The particle size in the unfractionated ferrofluid is 11.3 nm.

the values of α and λ are comparable to the values derived in section 3.1. The relative decrease nevertheless strongly depends on λ, the effective value of which is difficult to obtain for the polydisperse ferrofluid used here. Moreover, as will be shown further on, phase separation causes severe fractionation of magnetic particle sizes. Fractionation is not considered in the mean field calculations but can be expected to have a noticeable influence on the phase behavior.

3.6. Size Fractionation upon Phase Separation. Figure 13 shows the low concentration part of the phase diagram of FFR (Figure 7), with the magnetic particle diameter d_M in the gas phase at several points on the gas lines. The figure clearly shows that forcing a sample deeper into the two-phase region drives large particles into the concentrated phase.

Fractionation will cause a discrepancy between the true colloid concentration $c_{col,true}$ and the"experimental"colloid concentration $c_{col,exp}$ calculated from the susceptibility χ_i. To see how c_{col} is affected, we first write it as $c_{col} = n\langle M_p\rangle$, where $n = N/V$ is the number density of particles and $\langle M_p\rangle$ is the number average mass of a single particle. Because of the high mass density ρ_m of magnetite, $\langle M_p\rangle$ will be mainly determined by the magnetite core: $\langle M_p\rangle \approx \langle V_m\rangle\rho_m \propto \langle d_m{}^3\rangle$ (V_m and d_m are the core volume and diameter, respectively). In the low concentration regime, eq 6 holds and the number density is $n \propto \chi_i/\langle m^2\rangle \propto \chi_i/\langle d_m{}^6\rangle$. Note that the physical diameter is taken to be equal to the diameter of the magnetic core, which implies that the presence of a magnetically "dead" surface layer is neglected. The colloid concentration therefore depends on χ_i as

$$c_{col} = k\chi_i \propto d_M^{-3}\chi_i \qquad (13)$$

where $d_M{}^3 = \langle d_m{}^6\rangle/\langle d_m{}^3\rangle$ is the same as used in eq 2. It is clear from (13) that the proportionality constant k strongly depends on the particle size distribution. However, in the experiments k is only determined from unfractionated samples and is taken constant. The relation between the experimental and true concentration is therefore

$$c_{col,true} = k\chi_i = \frac{d_{M,0}{}^3}{d_M{}^3}k_0\chi_i = \frac{d_{M,0}{}^3}{d_M{}^3}c_{col,exp} \qquad (14)$$

where k_0 and $d_{M,0}$ denote the values obtained from homogeneous and hence unfractionated samples. Equation 14 can be directly related to Figure 13, where d_M is displayed for phase-separated samples. It can be seen that the true colloid concentration can be as much as 3.5 times as high as the experimental concentration ($d_{M,0}/d_M = 11.3/7.4$).

A clear effect of fractionation is the strange shape of the liquid lines in Figure 10 of samples with a high polymer/

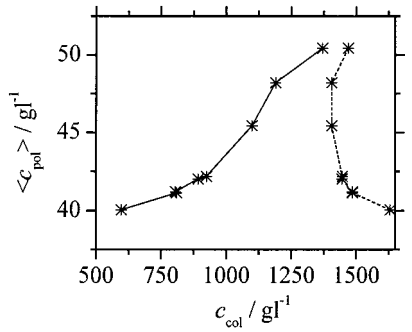

Figure 14. "C-shaped" liquid line (dashed) in phase diagram turns into a monotonically increasing line (solid) after correcting for fractionation upon phase separation.

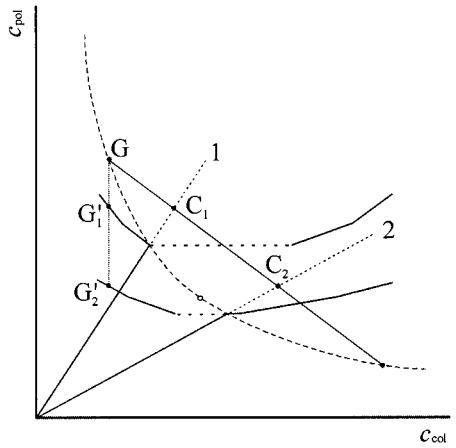

Figure 15. Reconstruction of the phase diagram and node lines.

colloid ratio. These lines were expected to be monotonically increasing but are in fact "C-shaped" due to an overestimation of the colloid concentration in the liquid phase. The overestimation is most pronounced if the absolute amount of magnetic material in the liquid phase is small; in the most extreme case, an apparent colloid concentration of 2284 g L^{-1} was found, corresponding to a volume fraction of 79%.

To illustrate the effect of fractionation, one of the liquid lines in Figure 7 was recalculated with a correction for the effect of fractionation on the measured colloid concentration of the corresponding gas phase. Thus, c_{gas} in (12) was corrected using (14) and the magnetic diameters shown in Figure 13. Correcting the liquid line in this way indeed results in a monotonically increasing line, as can be seen in Figure 14. Note that the point at the lowest polymer concentration in this figure is shifted toward a 63% lower colloid concentration.

3.7. Reconstruction of the Phase Diagram. The construction method for monodisperse components, described in section 3.4, can also be reversed: the real coexistence curve and node lines can be reconstructed by combining two experimental gas lines or liquid lines. Consider, as illustrated in Figure 15, two points G_1' and G_2' on the gas lines of samples 1 and 2. If the colloid concentrations on G_1' and G_2' are equal, both these points correspond to the end of one node line. Therefore, their initial compositions C_1 and C_2 must also be part of that same node line. Knowing this, the point G can be located on the intersection between the line through G_1' and G_2' and the node line through C_1 and C_2. This reconstruction method contains no assumptions and can be applied to any two-component mixture where the concentration of only one of the components can be determined directly. Incidentally, our method resembles a previously used method[28] to construct phase diagrams of mixtures of colloids and nonadsorbing polymer using only the total composition and the volume ratio of the coexisting phases.

Unfortunately, straightforward application of this reconstruction method to Figure 7 did not lead to satisfactory results. First, node lines obtained by combining two experimental gas lines at several colloid concentrations crossed each other within the two-phase region. This is, of course, physically impossible. And second, all node lines determined at a certain colloid concentration from different sets of gas lines should overlap. This was not the case: the node lines were not even parallel. The main reason is that size fractionation causes a drastic change in the relation between F and c_{col}, which was assumed to be constant (see previous section). Since particles in the dilute phase are smaller than average, the colloid concentration calculated from F is smaller than the true concentration. In some cases, the difference is as high as a factor of 3. Furthermore, since fractionation is different for each sample, two gas lines that are combined at the same value of F actually have different colloid concentrations. And finally, the reconstruction method cannot be applied to systems with polydisperse components, because in such systems the two-phase region is separated from the homogeneous mixture by a multidimensional coexistence *surface* rather than a curve in a two-dimensional plane.

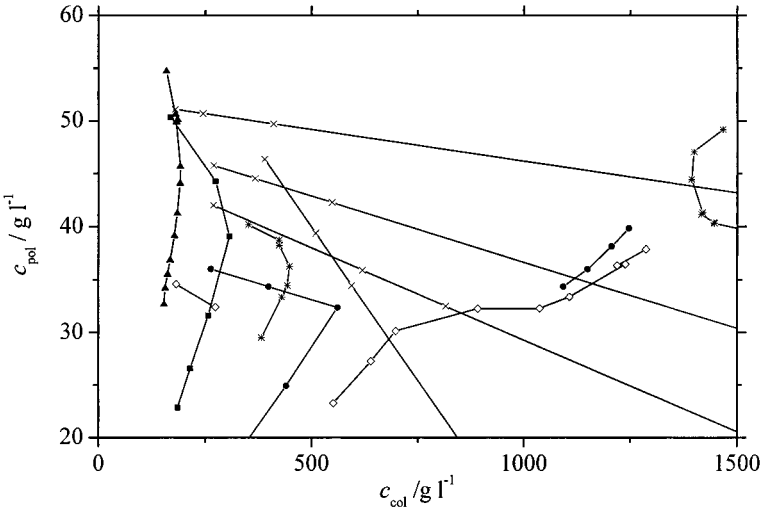

Figure 16. Phase diagram of FFR, with node lines.

To minimize the influence of polydispersity, we reconstructed the phase diagram focusing on those parts of the gas lines where the least fractionation was found, i.e., close to the coexistence curve. To this end, only combinations of samples with comparable polymer/colloid ratios were used for reconstruction. Points between measurements were found by cubic spline interpolation. The results in Figure 16 show that three out of four node lines do not cross within the two-phase region, but one node line has a slope which differs significantly from the others and crosses all others node lines. Because there are almost no points on liquid lines with the same colloid concentration, the end points at the liquid side of the node lines could not be obtained.

4. Conclusions

In this paper, a susceptibility meter based on a Colpitts oscillator has been described and tested. With this instrument, phase instabilities of magnetic fluids containing free polymer were investigated. With an increase in the amount of polymer, phase separation can be induced without a magnetic field at polymer concentrations as low as 30 g L^{-1}. In an applied magnetic field, phase separation occurs at lower polymer concentrations, but phase separation in the absence of polymer was never found. Excess oleic acid was also found to destabilize the ferrofluid.

Furthermore, an exact method for reconstructing the coexistence curve and node lines was described and tested. Although size fractionation hampered the reconstruction of node lines, the experimental phase diagram qualitatively agrees with expectations.

Acknowledgment. We thank Dr. L. Vékás and Dr. D. Bica for providing FFR and I. Dolbnya, R. van Tol, and E. Homan for their assistance with SAXS measurements at the DUBBLE beamline.

LA011117J

(28) Bodnár, I.; Oosterbaan, W. D. *J. Chem. Phys.* **1997**, *106*, 7777.